CONF-920913--26

PREPARED FOR THE U.S. DEPARTMENT OF ENERGY,
UNDER CONTRACT DE-AC02-76-CHO-3073

PPPL-2889
UC-420,421,423,424,426

PPPL-2889

DISRUPTIONS IN THE TFTR TOKAMAK

BY

A. JANOS, E.D. FREDRICKSON, K. McGUIRE, ET AL.

MARCH, 1993

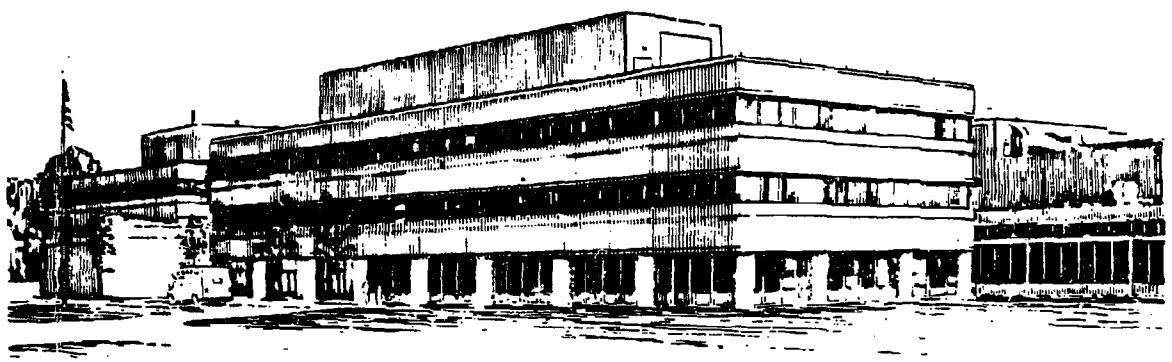

PRINCETON UNIVERSITY, PRINCETON, NEW JERSEY

This is a preprint of a paper presented at the Fourteenth International Conference on Plasma Physics and Controlled Nuclear Fusion Research, September 30 through October 7, 1992 in Wurzburg, Germany.

PPPL--2889

DE93 011497

INTERNATIONAL ATOMIC ENERGY AGENCY

FOURTEENTH INTERNATIONAL CONFERENCE ON PLASMA PHYSICS AND CONTROLLED NUCLEAR FUSION RESEARCH

Würzburg, Germany, 30 September – 7 October 1992

IAEA-CN-56 / A-7-15

DISRUPTIONS IN THE TFTR TOKAMAK [1]

A. Janos, E. D. Fredrickson, K. McGuire, S. H. Batha, M. G. Fell, M. Bitter, R. Budny, C. E. Bush, P. C. Efthimion, R. J. Hawryluk, K. W. Hill, J. Hosea, F. C. Jobes, D. W. Johnson, F. Levinton, D. Mansfield, D. Meade, S. S. Medley, D. Monticello, D. Mueller, Y. Nagayama, D. K. Owens, H. Park, W. Park, D. E. Post, J. Schivell, J. D. Strachan, G. Taylor. M. Ulrickson, S. von Goeler, E. Wilfrid, K. L. Wong, M. Yamada, K. M. Young, M. C. Zarnstorff, S. J. Zweben, and the TFTR Group

Princeton Plasma Physics Laboratory
Princeton University
Princeton, N.J. 08543
United States of America

J. F. Drake and R. G. Kleva

Plasma Fusion Center
University of Maryland
College Park, Maryland
United States of America

H. H. Fleischmann

Applied and Engineering Physics
Cornell University
Ithaca, New York 14853
United States of America

[1]Supported by U.S. DoE Contract No. DE-AC02-76-CHO-3073

Disruptions in the TFTR Tokamak

Abstract

For a successful reactor, it will be useful to predict the occurrence of disruptions and to understand disruption effects including how a plasma disrupts onto the wall and how reproducibly it does so. Studies of disruptions on TFTR at both high-β_{pol} and high-density have shown that, in both types, a fast growing m/n=1/1 mode plays an important role. In high-density disruptions, a newly observed fast m/n = 1/1 mode occurs early in the thermal decay phase. For the first time in TFTR, q-profile measurements just prior to disruptions have been made. Experimental studies of heat deposition patterns on the first wall of TFTR due to disruptions have provided information on MHD phenomena prior to or during the disruption, how the energy is released to the wall, and the reproducibility of the heat loads from disruptions. This information is important in the design of future devices such as ITER. Several new processes of runaway electron generation are theoretically suggested and their application to TFTR and ITER is considered, together with a preliminary assessment of x-ray data from runaways generated during disruptions.

1. PRECURSORS

Studies of disruptions on TFTR have been done at high-β_{pol} and high-density, using a fast electron cyclotron emission (ECE) grating polychrometer for the electron temperature profile, two soft x-ray cameras and a Mirnov array. While there are important differences, a fast growing m/n=1/1 mode is found to play an important role in both types of disruptions.

The precursor in hot, high-β_{pol} plasmas on TFTR is an m/n = 1/1 mode [1,2]. Reconstructions indicate that it has a kink-like (rather than island-like) structure. This precursor has a very rapid growth rate, often $>10^3$ s^{-1}. A large, non-thermal burst of ECE emission lasting 100-200 μs is observed before the thermal transport phase, which is a rapid (≈200 μs), structureless collapse of the T_e profile.

Minor and major disruptions at moderate-to-high density are initiated by an m/n=1/1 "cold bubble" structure moving into the plasma core (Fig. 1), resembling the "vacuum bubble" model of disruptions first proposed by Kadomtsev and Pogutse [3]. The growth rate of the precursor ($\gamma \approx 5 \times 10^3$ s^{-1}) is about the same as that for the high-β_{pol} disruptions. At these growth rates, the growth time is only ≈ 1 ms compared to the total disruption time of the order of 100 ms. For the minor disruption, the measured Λ ($\equiv \beta_{pol}^{equil} + l_i/2$) remains unchanged, suggesting no change in the internal inductance. For the major disruption, Λ is seen to decrease sharply, at the end of the crash phase, suggesting a redistribution of current. The change in Λ from 1.15 to 0.85 is consistent with a flattening of the current profile to the q≈3 radius ($\beta_{pol} \approx 0.1$ at this time). This suggests that either the m=1 mode or other modes excited during the crash lead to a reconnection or a destruction of the magnetic flux surfaces and a broadening of the current profile. A possible explanation for the difference between the minor and major disruptions is that for the major disruption the formation of the bubble is driven by a quasi-external kink whereas for the minor disruption the precursor is categorized as an internal kink. This hypothesis is supported by comparison of the effective resistive timescale to the bubble growth timescale [2,4].

For reactor plasmas and ITER, active external feedback control will be difficult in either case because of the fast growing nature of the instability. Also, the high density disruption

studies suggest that active control of the edge temperature might be used to prevent the major disruption.

2. q-PROFILE MEASUREMENTS PRIOR TO DISRUPTIONS

For the first time in TFTR, q-profile measurements were made prior to disruptions using the Motional Stark Effect (MSE) diagnostic [5]. Absolute error is 0.15 and relative error is 0.03 with a time resolution of 5 ms. It has not been possible to obtain data throughout the disruption and into the current-quench phase since MSE measures the Stark shift of line emission from neutral-beam particles and it has been standard practice up to now to turn the beams off when a disruption occurs. Figure 2 shows how, in a high-β_p discharge with neutral-beam heating of 10 MW for 2 s, q(0) starts to increase about 200 ms just before the disruption, from ≈ 0.94 to >1.02. Simulations from TRANSP using neoclassical resistivity show qualitative agreement of the q(0) time evolution. Up until 9.5 ms before the thermal quench of the disruption begins, the profiles are little changed.

3. FIRST WALL HEAT LOAD DISTRIBUTION

The primary power handling surface for TFTR is a bumper limiter on the small-major-radius side representing a large part (23%) of the first wall (360° toroidally, ±60° poloidally with respect to the midplane). It is comprised of 1920 carbon or carbon-composite tiles and is divided into 20 bays toroidally, corresponding to the 20 toroidal field coils. A unique feature of TFTR is that this limiter is instrumented with a large number of thermocouples (100) in a 2-D regular grid pattern. This extensive array provides a map of the bulk tile temperature before and after each discharge [6]. By comparing the rise in temperature (ΔT) due to appropriate individual discharges (e.g., with and without disruptions), the heating effects due to specific events (e.g., disruptions) are determined. (The bulk tile cooling time >> the heat deposition [discharge] time.) A 1°C rise of the entire limiter corresponds to ≈0.84 MJ.

There are large reproducible toroidal and poloidal variations in the measured heat loads even in non-disruptive discharges (Fig. 3a). Generally, hot areas are either areas closer to the plasma (deviations of the order of 2 mm significantly affect the heat loads) or areas which receive extra heating due to neighboring recesses in the wall [6,7].

Disruptive Discharges:

Disruptions preferentially heat the same areas (Fig. 3b) which are heated during discharges without disruptions (Fig. 3a). Not all the same spots may be heated since disruptive discharges tend to collapse in major radius, thus predominantly heating the high spots near the midplane. In addition to these predictable areas, however, there are sometimes unexpected areas of heating which vary from disruption to disruption, even for disruptions of the same type and under comparable device conditions.

Discharge 45283 disrupts during the I_p ramp-down ($I_p \approx 1.1$ MA) and may be compared to discharge 45282 which is only one discharge before, thus minimizing differences due to long-term conditioning or changes in operation mode. Both discharges are ohmically heated with plasma currents of $I_p = 1.8$ MA and have major radii of R = 2.45 m. For the disruption energy alone, the maximum ΔT of 29°C corresponds to 12.7 kJ deposited in one tile or 1.2 MJ/m^2. For this ohmic disruption, assuming that half of the energy is deposited during the thermal quench time of ≈ 2 ms, the power loading would be 310 MW/m^2. For comparison, the power loading for a non-disruptive discharge with 20 MW of neutral beam power is only ≈ 1 MW/m^2.

Poloidal profiles of ΔT for the non-disruptive discharge (Fig. 4a) are generally peaked around the midplane, as expected for R = 2.45 m since the minor radius of the plasma is smaller than the radius of curvature of the limiter. The profile for the disruption portion only (Fig. 4c) looks qualitatively similar except that it has a stronger peak on the midplane. The average ΔT for the disruption portion of the discharge was 60% higher than for the non-disruptive discharge; however, the maximum ΔT for the disruption was >3 times that for the non-disruptive discharge. We characterize the spatial variations in ΔT by defining [8] a peaking factor in the toroidal direction, as a function of poloidal angle, ϑ, as

$$f_{peak}(\vartheta) \equiv \text{Max } \Delta T(\vartheta) \,/\, \text{Avg } \Delta T(\vartheta).$$

Peaking factors are important in the design of future devices such as ITER. In the vicinity of the midplane, where most of the energy is deposited, peaking factors for the heat load due to a disruption range from 2 to 5 (Fig. 5), only slightly higher than for non-disruptive discharges (2 to 4). Away from the midplane, peaking factors for the disruption heat load can exceed 25, although the heat load in these areas is usually less than near the midplane.

Locked modes much more significantly redistribute the heat load from disruptions than any discharge-to-discharge variations (Fig. 6). Locked modes always alter the heating pattern in TFTR, creating helical patterns which clearly match the expected trajectories based on the m/n mode numbers. Figure 6 shows a 1.2 MA, $q(a) \approx 4$, ohmically heated discharge which suffered a m/n = 4/1 locked mode before disruption (at 0.5 MA) during the current ramp-down. Locked modes make what were the coldest areas into the hottest areas, heating areas which are very rarely heated, and vice versa. Mirnov coil data and tomographic analysis reveals that the high heat flux paths on the limiter lie near the X-points of the mode. Tomographic analysis also reveals that the plasma shape is distorted due to the mode, with the plasma extending closer to the wall at the X-points. In discharges with rotating modes, the heat is distributed in a more toroidally symmetric pattern. Peaking factors for locked mode disruptions are significantly enhanced compared to either peaking factors for non-disruptive discharges or peaking factors at the midplane for disruptive discharges. Peaking factors range from 2 through 10, and are large ($\approx$ 10) even near the midplane.

Even in the case of locked modes which originate from q surfaces deep inside the plasma, perturbed heat patterns are observed on the wall. A high current discharge (I_p = 1.6 MA, B_{TF}=4.9 T, R=2.45 m, q(a) = 4.5) with high neutral-beam heating power (P_{NB}=22 MW) was observed to develop a m/n = 2/1 locked mode during beam injection. A helical heating pattern developed on the wall, but to a lesser extent compared to the m/n=4/1 case above.

By causing an unusually high deposition of heat in normally cold areas which may not be sufficiently conditioned for the large heat fluxes, large influxes of impurities come from the walls. This is evidenced by the difficulty in producing discharges after a disruption and by the oxygen dominated discharges which are finally produced following a disruption.

The limiter heating profiles for low-q disruptions are similar to those for the ramp-down disruption above. Intentional low-q ($1.95 < q < 2.5$) disruptions, created to condition the limiter of TFTR, are produced by rapidly moving the plasma onto the bumper limiter at constant I_p. The disruption increased the total wall loading to more than five times that of similar discharges where R was decreased nearly to the point of disruption and then increased to the point where the plasma was not limited by the bumper limiter. The peaking factor for the disruptive portion alone ranges from 2 to 5, similar to that for the ramp-down disruption.

In contrast to low-q disruptions, high-density disruptions generally result in very little additional heating compared to that from companion discharges which have nearly the same time

evolution (e.g., I_p, R, P_{in}). Often the disruptive discharge produces less average heating and lower peak temperatures. This suggests that there are significant differences between the two discharges in the balance between radiated power and power conducted to the bumper limiter along field lines. Radiated power heats not only the bumper limiter but also the rest of the wall. These differences may contribute to the onset of the disruption in one discharge and not the other. High-density disruptions also often created hot spots, but fewer in number than from other types of disruptions. In general, results were similar for both ohmically-heated and neutral-beam-heated discharges.

For ITER, the general predictability of the distribution of the heat load is a benefit. However, the occasional variability and the unexpected heat pattern from locked mode disruptions may pose problems. A tentative characterization of disruptions for a representative ITER scenario [8] assumes peaking factors of 5 on the first wall (not the divertor), which is on the high end of peaking factor values actually measured in TFTR in general. However, measured peaking factors from locked mode disruptions can be much larger (x2) than typical disruption design values for ITER. The same design includes the possibility of a peak energy load on the first wall of 5 MJ/m^2, more than four times that for the disruption above. Based on energy loads during the thermal quench of 2 MJ/m^2 over quench times of 0.1-3.0 ms [8], the power loads would be 670 MW/m^2 - 20 GW/m^2, much greater than that of the experimental example above.

4. FAST, BUMPER LIMITER SURFACE TEMPERATURE MEASUREMENTS

In addition to the bulk tile temperature measurements described in the previous section, fast surface-temperature measurements are made of the bumper limiter tiles using a 15-channel poloidal array of fast (200 kHz) IR detectors which cover ± 30 ° poloidally with respect to the midplane. Each channel has a beam splitter and two silicon diodes (0.9 and 1.0 μm band pass filters), permitting two color pyrometry.

The local surface temperature from a typical high current disruption (Fig. 7) can rise from < 625 °C to > 1250 °C in ≈ 100 μs near the midplane during the thermal quench phase. The maximum heat load to the surface, calculated from the time history of the temperature, was 2 MJ/m^2 integrated over the entire disruption time, slightly less than twice that measured for the ramp-down disruption example above. The average heat flux was ≈ 200 MW/m^2, slightly less than that measured for the example above, while the peak (in time) heat flux was ≈ 500 MW/m^2

5. RUNAWAY ELECTRONS

In view of the experimental observation of strong runaway electron beams during disruptions in tokamaks [9] and the projected serious wall damage potential for large tokamaks [10] and for ITER in particular, an effort to study runaways in disruptions was initiated.

5.1 Theoretical Analysis

Using the presently accepted disruption model [2,11] and typical plasma parameters (j and n_e in the disruption are assumed to equal their pre-disruption values and T_e in the final phase is assumed to be ≈10 eV), this analysis indicated that three different runaway sources, including two not normally considered previously, can be effective in large (several MA) tokamaks [12]: 1) The well known Dreicer-type generation through evaporation of runaways from the thermal distribution is found to generate beams carrying a sizeable fraction of the original current in existing tokamaks (TFTR, JET) and, in particular, in high-current low-to-medium n_e discharges. 2) Trapped high-energy thermal electrons from the original discharge surviving the thermal quench will runaway whenever they become untrapped after re-closure of the magnetic surfaces.

Analyzing the collisional decay of trapped-electron populations [13] and recognizing that a trapped density of only $(10^{-3} - 10^{-4}) \times n_e$ will be sufficient to generate beams carrying the full pre-disruption j, we find that this process will be limited by the time needed for re-closure of the magnetic surfaces. Assuming 1-2 ms after the thermal quench, this process will be effective by itself mainly in high-T_e, low-to-medium-n_e disruptions. Both of the above processes will be self-quenching because of a reduction in the resistive E-fields resulting from the increasing runaway currents, and both of the above processes will be completed during the first 0.5 - 1.0 ms after the thermal quench. 3) Close collisions of any existing runaways with the cold plasma electrons can transfer recoil energies exceeding E_{crit} of the Dreicer theory, and most of these recoil electrons will run away [14]. Such avalanching will lead to an exponential growth of any runaway population during the current quench phase. Using Coulomb cross sections, the exponentiation time will equal the time needed for relativistic runaways to gain 10-20 MeV from E, independent of plasma parameters; assuming sufficient runaway confinement for large tokamaks, the runaway population will grow by an order-of-magnitude per 1-1.5 MA decrease in total discharge current. In TFTR and JET, this process may lead to significant enhancement factors of $10 - 10^4$. Analysis of TFTR data for comparison to this theoretical analysis is in progress.

In ITER, it is expected that the Dreicer-type generation process will be limited mainly to n_e significantly below presently projected values. The third process of runaway generation can be dominant in ITER with avalanche enhancement factors of up to 10^{10}-10^{14}. Thus, a few runaway electrons per cm^3 can lead to beams carrying a sizable fraction of the pre-disruption current.

5.2 Experimental Analysis

This study was initiated with a statistical analysis of data from three hard x-ray 3" NaI(Tl) flux monitors located on the different walls of the TFTR bay, nearly at the midplane level. Wide statistical fluctuations in the amplitude and time dependence for any given discharge as well as between discharges resulted. Such fluctuations might be expected in view of the strongly forward-focussed distribution of bremsstrahlung x-rays produced by multi-MeV electrons and the expected variation in the impact position at the wall. Also, such fluctuations are consistent with the observation that heat loads also show some variations.

In disruptions without current tails, major x-ray bursts are observed when the current has decayed to 10-30%; leakage of runaways during the earlier part of the current quench phase is not observed. In disruptions with current tails, x-ray bursts tend to appear near the transition to the tail. Thereafter, less emission is observed during the slow tail decay followed by a stronger signal at the final drop-off. In some cases, no significant emission is observed during the tail decay. X-ray bursts sometimes are observed just before the current spike at the beginning of disruptions, indicating the loss of runaways already existing. Statistics are given in Table 1 for various levels of I_p. Correlation analysis of the features and discharge parameters is in progress.

6. SUMMARY

In TFTR, data suggests that the m/n = 1/1 mode plays an important role in both high-β_{pol} and high-density disruptions. For the first time, a fast m/n = 1/1 "cold-bubble" precursor to high-density disruptions has been experimentally observed. In TFTR with a large surface area limiter, disruptions generally deposit energy on the same first wall areas that receive the most energy during non-disruptive discharges. These areas are usually closer to the plasma or are unshielded by neighboring areas. However, there is some variability to the heat deposition from disruptions which would make protection of only selected areas less effective in preventing damage. While most of the heat is deposited near the midplane during disruptions, where peaking factors $f_{peak}(\vartheta) \equiv \text{Max } \Delta T(\vartheta) / \text{Avg } \Delta T(\vartheta)$ can be on the order of 2 to 5, a significant

amount of energy can be deposited in areas further from the midplane where the peaking factor can exceed 25. Tentative peaking factors for the first wall (not the divertor) for disruptions in ITER, based on a characterization of disruptions for a representative ITER scenario [8], have been assumed to be of the order of 5, similar to those measured in the vicinity of the midplane for disruptions on TFTR. However, locked modes in particular significantly alter the heat load pattern due to disruptions and result in peaking factors twice as large. The heat load to the wall expected for ITER during disruptions is several times the ≈ 1 MJ/m^2 for the TFTR example described above, while the expected power flux is much greater than the ≈ 300 MW/m^2 for the TFTR example. In addition, different types of disruptions show significant differences in wall loading. Potential sources of electron runaway generation in TFTR have been investigated; data from x-ray detectors show large differences from detector to detector and from discharge to discharge, consistent with the probable runaway source of the x-rays.

Acknowledgements - This work was supported by U.S. DoE Contract No. DE-AC02-76-CHO-3073.

References

[1] E. D. Fredrickson, *et al.*, IAEA, Washington, D.C. Oct. 1990; A. C. Janos, E. Fredrickson, M. Corneliussen, *et al.*, J. Nucl. Mater. 176&177 (1990) 773-778.
[2] E. D. Fredrickson, *et al.*, PPPL Report 2785, Jan. 1992, submitted to Nucl Fusion (July 7, 1992).
[3] B. B. Kadomtsev and O. P. Pogutse, Sov. Phys. JETP 38 (1974) 283.
[4] R. G. Kleva, J. F. Drake, Phys. Fluids B 3 (1991) 372.
[5] F. M. Levinton, PPPL-2853, Rev. Sci. Instru., to be published, 1992; F. M. Levinton *et al.*, Phys. Rev. Lett. 63 (1989) 2060.
[6] A. Janos, M. Corneliussen, E. Fredrickson, *et al.*, Rev. Sci. Instrum. 61 (Oct., 1990) 2973-2975.
[7] G. W. Barnes *et al.* in: Proc. of the 13th Symposium on Fusion Engineering (Knoxville, Oct. 1989).
[8] D. Post, private communication; ITER Physics, ITER Physics Documentation Series 21 (IAEA, Vienna, 1991) 171-185.
[9] O. N. Jarvis, G. Sadler, and J. L. Thompson, Nucl. Fusion 28 (1988) 1981; H. Takatsu *et al.*, Proc. Symposium on Nuclear Fusion Technology, Tokyo (1988).
[10] K. A. Niemer, C. D. Groessmann, J. G. Gilligan, and H. H. Bolt, Proc. 13th Symposium on Fusion Engineering, Knoxville, TN, October 1989, p.941; A. J. Russo, Nucl Fusion 31 (1991) 117.
[11] J. A. Wesson, *et al.*, Nucl. Fusion 29 (1989) 641; K. M. McGuire *et al.*, J. Nucl. Mater. 121 (1984) 329.
[12] H. H. Fleischmann. S. J. Zweben *et al.*, to be published.
[13] R. F. Post, Nucl. Fusion 27 91987) 1577.
[14] R. Jayakumar, H. H. Fleischmann, and S. J. Zweben, PPPL-2849.

Figures

1. Profiles of the electron temperature and soft x-ray emissivity at the beginning of a major disruption of a low q(a) discharge [q(a) = 2.5, a = 0.8 m, $\langle n_e \rangle \approx 4.5 \cdot 10^{19}$ m^{-3}, R = 2.45 m, I_p = 2.5 MA, and B_T = 5.21 Tesla]. Profiles d, e, and f correspond to the same time in the two figures. There is 50 μs between profiles.

2. q-profile and q(0) measurements prior to a disruption. Time resolution is 5 ms. Profiles are at t = 4.0025, 4.2525, and 4.5275 s, the last being 10 ms before the start of the current quench phase of the disruption.

3. Temperature rise maps of the bumper limiter in TFTR due to a pair of discharges which are similar in all discharge parameters except that one does not disrupt and the other does. (a) Non-disruptive discharge. (b) Disruptive discharge. (c) Mechanically measured deviation of the tiles at the midplane from a circle of constant radius of 165.1 cm after the discharges above.

4. Profile of temperature change ΔT versus poloidal angle ϑ for (a) Non-disruptive discharge, (b) Disruptive discharge, and (c) Disruptive portion alone (Difference between the non-disruptive and the disruptive discharge.) Includes the maximum ΔT at a given ϑ and the average ΔT as a function of poloidal angle; the RMS deviation from the average, at a given ϑ, is indicated by the bars.

5. Peaking Factor profiles versus poloidal angle for (a) Non-disruptive discharge, and (b) Disruptive portion only of a disruptive discharge.

6. Heat load distribution for an ohmic discharge with an m/n = (4,1) locked mode The expected trajectory of an m/n = (4,1) mode is superimposed.

7. Fast measurements of surface-temperature rise of bumper limiter tiles.

Table I

Statistics of X-Ray Signals
during High Current Disruptions
("current flat top" disruptions only)

Discharge Current (MA)	Number of Disruptions: Total	> 10 ms Tail (%)	Sizable X-Ray Signals (%)
> 1.0	62	37	85
> 1.5	26	50	100
> 2.0	3	67	67

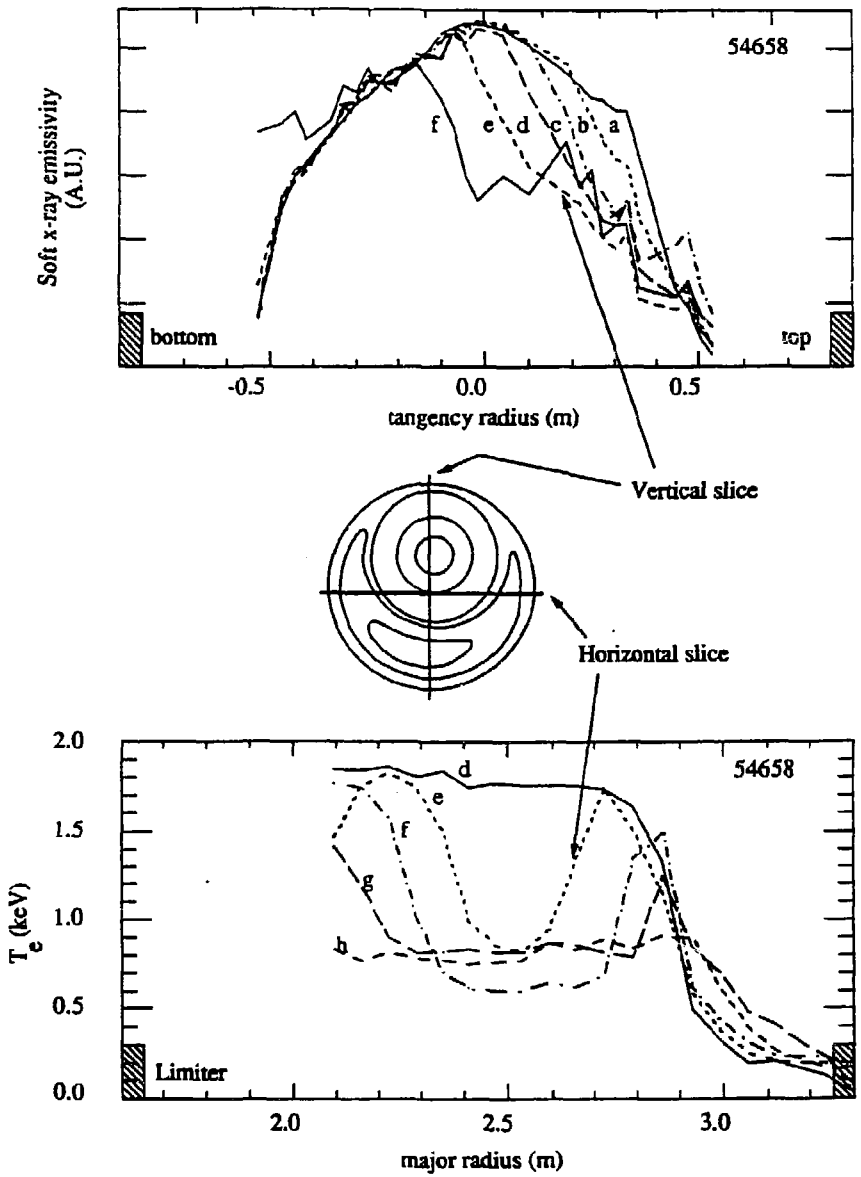
54658
f
e
d
c
b
a
Soft x-ray emissivity (A.U.)
bottom
top
-0.5
0.0
0.5
tangency radius (m)
Vertical slice
Horizontal slice
2.0
1.5
1.0
0.5
0.0
T_e (keV)
54658
d
e
f
g
b
Limiter
2.0
2.5
3.0
major radius (m)

Fig. 1

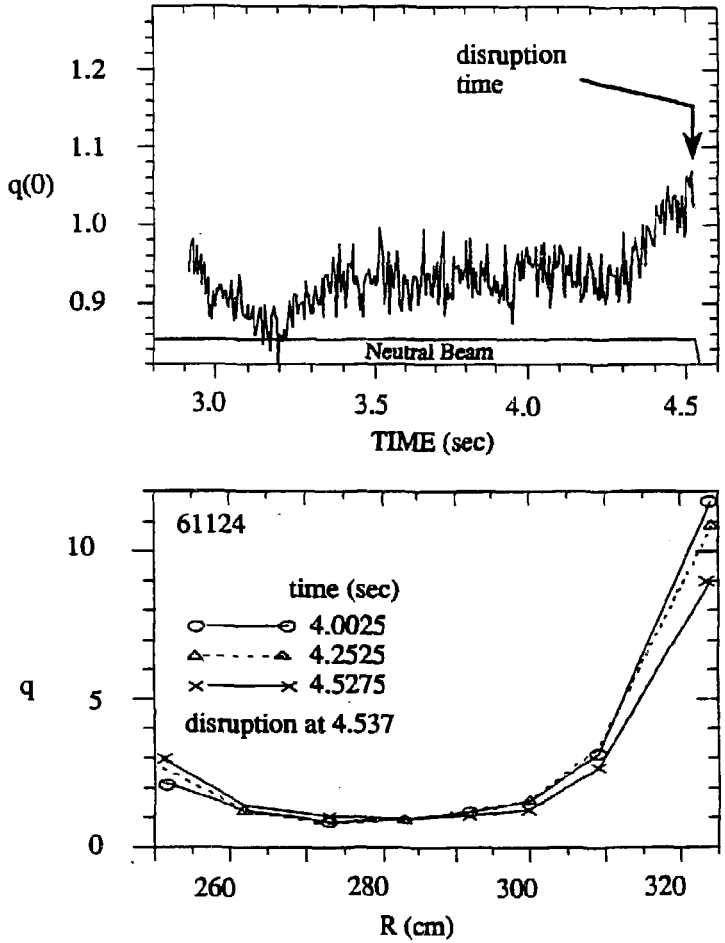
disruption
time
1.2
1.1
1.0
0.9
q(0)
Neutral Beam
3.0
3.5
4.0
4.5
TIME (sec)
61124
time (sec)
4.0025
4.2525
4.5275
disruption at 4.537
10
5
0
q
260
280
300
320
R (cm)

Fig. 2

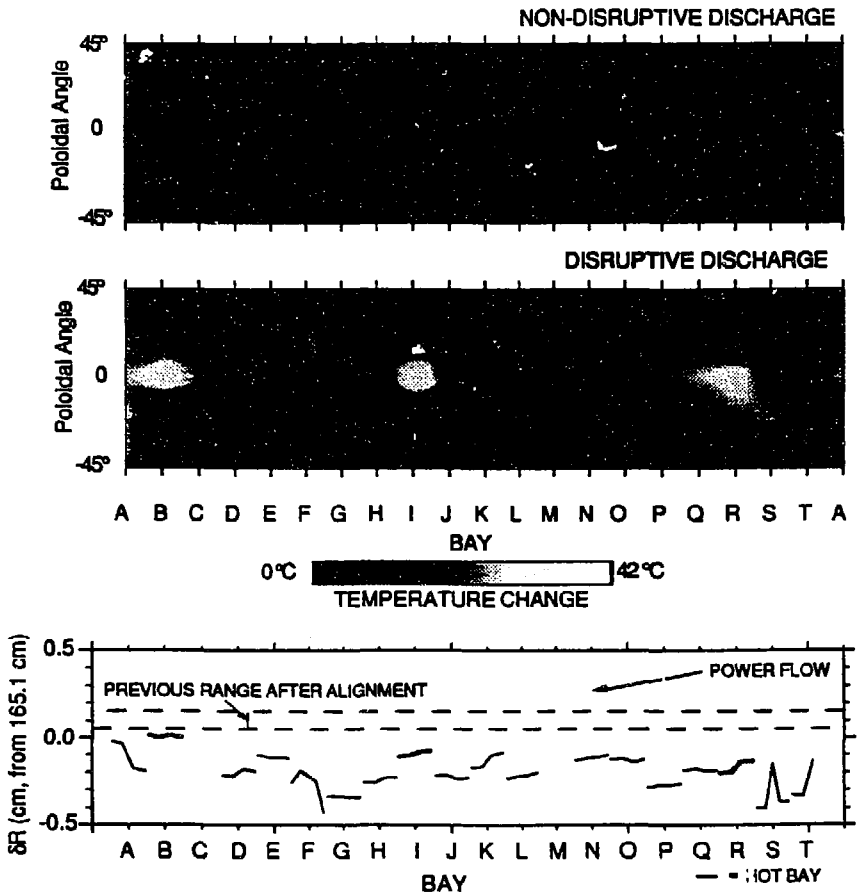
NON-DISRUPTIVE DISCHARGE
Poloidal Angle
45°
0
-45°
DISRUPTIVE DISCHARGE
Poloidal Angle
45°
0
-45°
A B C D E F G H I J K L M N O P Q R S T A
BAY
0°C
42°C
TEMPERATURE CHANGE
δR (cm, from 165.1 cm)
0.5
0.0
-0.5
PREVIOUS RANGE AFTER ALIGNMENT
POWER FLOW
A B C D E F G H I J K L M N O P Q R S T
BAY
HOT BAY

Fig. 3

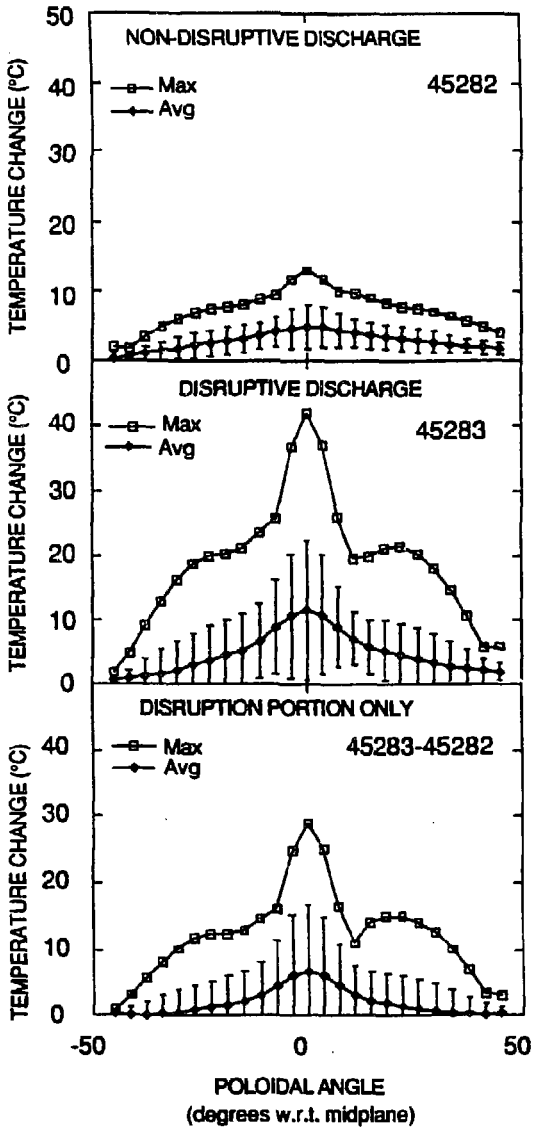
NON-DISRUPTIVE DISCHARGE
Max
Avg
45282
DISRUPTIVE DISCHARGE
Max
Avg
45283
DISRUPTION PORTION ONLY
Max
Avg
45283-45282
TEMPERATURE CHANGE (°C)
50
40
30
20
10
0
-50
0
50
POLOIDAL ANGLE
(degrees w.r.t. midplane)

Fig. 4

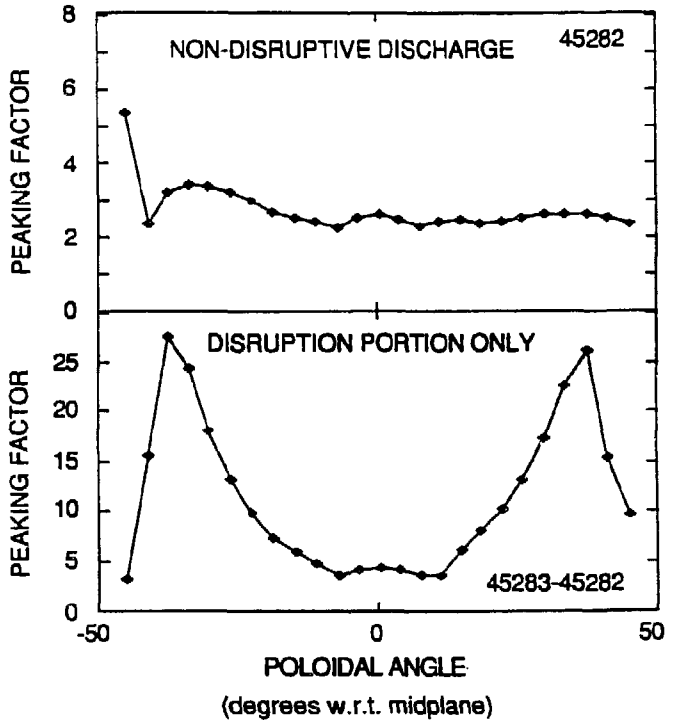
NON-DISRUPTIVE DISCHARGE
45282
PEAKING FACTOR
8
6
4
2
0
DISRUPTION PORTION ONLY
PEAKING FACTOR
25
20
15
10
5
0
45283-45282
-50
0
50
POLOIDAL ANGLE
(degrees w.r.t. midplane)

Fig. 5

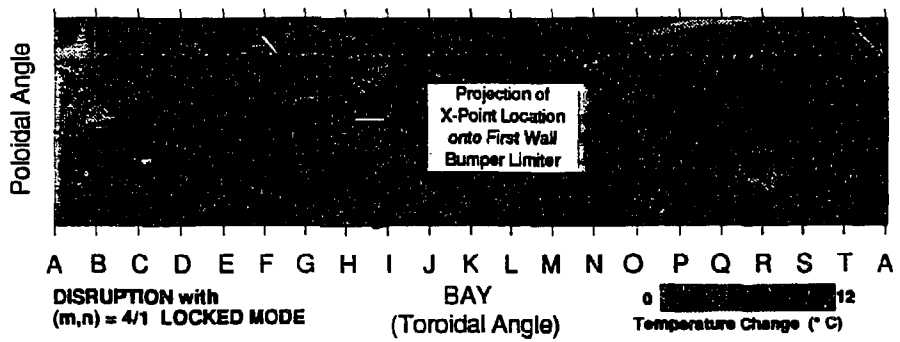
Poloidal Angle
Projection of
X-Point Location
onto First Wall
Bumper Limiter
A B C D E F G H I J K L M N O P Q R S T A
DISRUPTION with
(m,n) = 4/1 LOCKED MODE
BAY
(Toroidal Angle)
0
12
Temperature Change (° C)

Fig. 6

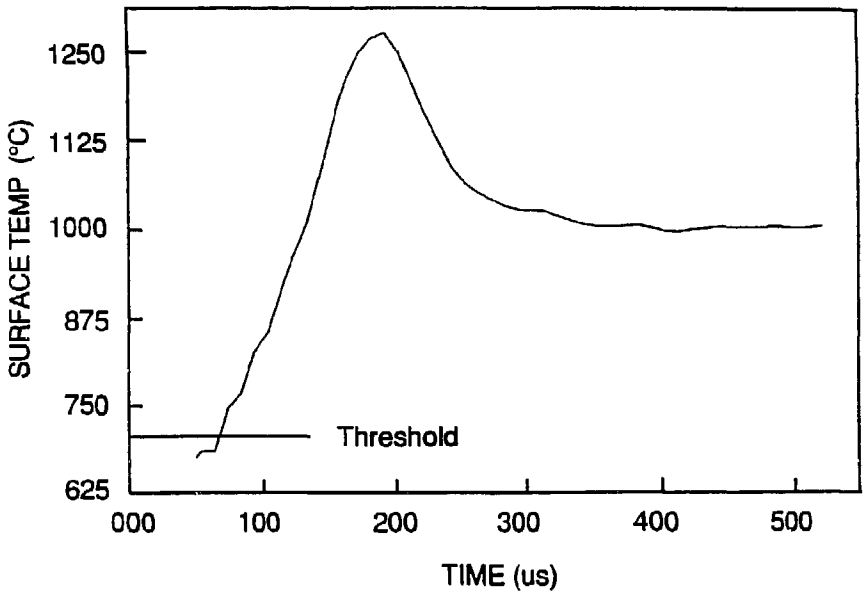
1250
1125
1000
875
750
625
SURFACE TEMP (°C)
Threshold
000
100
200
300
400
500
TIME (us)

Fig. 7

EXTERNAL DISTRIBUTION IN ADDITION TO UC-420

Dr. F. Paoloni, Univ. of Wollongong, AUSTRALIA
Prof. M.H. Brennan, Univ. of Sydney, AUSTRALIA
Plasma Research Lab., Australian Nat. Univ., AUSTRALIA
Prof. I.R. Jones, Flinders Univ, AUSTRALIA
Prof. F. Cap, Inst. for Theoretical Physics, AUSTRIA
Prof. M. Heindler, Institut für Theoretische Physik, AUSTRIA
Prof. M. Goossens, Astronomisch Instituut, BELGIUM
Ecole Royale Militaire, Lab. de Phy. Plasmas, BELGIUM
Commission-European, DG. XII-Fusion Prog., BELGIUM
Prof. R. Boucique, Rijksuniversiteit Gent, BELGIUM
Dr. P.H. Sakanaka, Instituto Fisica, BRAZIL
Instituto Nacional De Pesquisas Especiais-INPE, BRAZIL
Documents Office, Atomic Energy of Canada Ltd., CANADA
Dr. M.P. Bachynski, MPB Technologies, Inc., CANADA
Dr. H.M. Skarsgard, Univ. of Saskatchewan, CANADA
Prof. J. Teichmann, Univ. of Montreal, CANADA
Prof. S.R. Sreenivasan, Univ. of Calgary, CANADA
Prof. T.W. Johnston, INRS-Energie, CANADA
Dr. R. Bolton, Centre canadien de fusion magnétique, CANADA
Dr. C.R. James,, Univ. of Alberta, CANADA
Dr. P. Lukác, Komenského Universzita, CZECHO-SLOVAKIA
The Librarian, Culham Laboratory, ENGLAND
Library, R61, Rutherford Appleton Laboratory, ENGLAND
Mrs. S.A. Hutchinson, JET Library, ENGLAND
Dr. S.C. Sharma, Univ. of South Pacific, FIJI ISLANDS
P. Mähönen, Univ. of Helsinki, FINLAND
Prof. M.N. Bussac, Ecole Polytechnique,, FRANCE
C. Moutiet, Lab. de Physique des Milieux Ionisés, FRANCE
J. Radet, CEN/CADARACHE - Bat 506, FRANCE
Prof. E. Economou, Univ. of Crete, GREECE
Ms. C. Rinni, Univ. of Ioannina, GREECE
Dr. T. Mual, Academy Bibliographic Ser., HONG KONG
Preprint Library, Hungarian Academy of Sci., HUNGARY
Dr. B. DasGupta, Saha Inst. of Nuclear Physics, INDIA
Dr. P. Kaw, Inst. for Plasma Research, INDIA
Dr. P. Rosenau, Israel Inst. of Technology, ISRAEL
Librarian, International Center for Theo Physics, ITALY
Miss C. De Palo, Associazione EURATOM-ENEA , ITALY
Dr. G. Grosso, Istituto di Fisica del Plasma, ITALY
Prof. G. Rostangni, Istituto Gas Ionizzati Del Cnr, ITALY
Dr. H. Yamato, Toshiba Res & Devel Center, JAPAN
Prof. I. Kawakami, Hiroshima Univ., JAPAN
Prof. K. Nishikawa, Hiroshima Univ., JAPAN
Director, Japan Atomic Energy Research Inst., JAPAN
Prof. S. Itoh, Kyushu Univ., JAPAN
Research Info. Ctr., National Instit. for Fusion Science, JAPAN
Prof. S. Tanaka, Kyoto Univ., JAPAN
Library, Kyoto Univ., JAPAN
Prof. N. Inoue, Univ. of Tokyo, JAPAN
Secretary, Plasma Section, Electrotechnical Lab., JAPAN
S. Mori, Technical Advisor, JAERI, JAPAN
Dr. O. Mitarai, Kumamoto Inst. of Technology, JAPAN
J. Hyeon-Seok, Korea Atomic Energy Research Inst., KOREA
D.I. Choi, The Korea Adv. Inst. of Sci. & Tech., KOREA
Prof. B.S. Liley, Univ. of Waikato, NEW ZEALAND
Inst of Physics, Chinese Acad Sci PEOPLE'S REP. OF CHINA
Library, Inst. of Plasma Physics, PEOPLE'S REP. OF CHINA
Tsinghua Univ. Library, PEOPLE'S REPUBLIC OF CHINA
Z. Li, S.W. Inst Physics, PEOPLE'S REPUBLIC OF CHINA
Prof. J.A.C. Cabral, Instituto Superior Tecnico, PORTUGAL
Dr. O. Petrus, AL I CUZA Univ., ROMANIA
Dr. J. de Villiers, Fusion Studies, AEC, S. AFRICA
Prof. M.A. Hellberg, Univ. of Natal, S. AFRICA
Prof. D.E. Kim, Pohang Inst. of Sci. & Tech., SO. KOREA
Prof. C.I.E.M.A.T, Fusion Division Library, SPAIN
Dr. L. Stenflo, Univ. of UMEA, SWEDEN
Library, Royal Inst. of Technology, SWEDEN
Prof. H. Wilhelmson, Chalmers Univ. of Tech., SWEDEN
Centre Phys. Des Plasmas, Ecole Polytech, SWITZERLAND
Bibliotheek, Inst. Voor Plasma-Fysica, THE NETHERLANDS
Asst. Prof. Dr. S. Cakir, Middle East Tech. Univ., TURKEY
Dr. V.A. Glukhikh,Sci. Res. Inst. Electrophys.I Apparatus, USSR
Dr. D.D. Ryutov, Siberian Branch of Academy of Sci., USSR
Dr. G.A. Eliseev, I.V. Kurchatov Inst., USSR
Librarian, The Ukr.SSR Academy of Sciences, USSR
Dr. L.M. Kovrizhnykh, Inst. of General Physics, USSR
Kernforschungsanlage GmbH, Zentralbibliothek, W. GERMANY
Bibliothek, Inst. Für Plasmaforschung, W. GERMANY
Prof. K. Schindler, Ruhr-Universität Bochum, W. GERMANY
Dr. F. Wagner, (ASDEX), Max-Planck-Institut, W. GERMANY
Librarian, Max-Planck-Institut, W. GERMANY
Prof. R.K. Janev, Inst. of Physics, YUGOSLAVIA